Layer-Coupled States Facilitate Ultrafast Charge Transfer in a Transition Metal Dichalcogenide Trilayer Heterostructure

Peymon Zereshki,[†] Yaqing Wei,[‡] Run Long,[*,‡] and Hui Zhao[*,†]

[†]*Department of Physics and Astronomy, The University of Kansas, Lawrence, Kansas 66045, United States*

[‡]*College of Chemistry, Key Laboratory of Theoretical and Computational Photochemistry of Ministry of Education, Beijing Normal University, Beijing, 100875, People's Republic of China*

E-mail: runlong@bnu.edu.cn; huizhao@ku.edu

Abstract

Forming van der Waals multilayer structures with two-dimensional materials is a promising new method for material discovery. The weak van der Waals interlayer interaction without atomic correspondence relaxes lattice matching requirement and allows formation of high-quality interfaces with virtually any combinations of two-dimensional materials. However, the weak nature of the van der Waals interaction also makes it challenging to harness emergent properties of such multilayer materials. Previous studies have indicated that in transition metal dichalcogenide bilayer heterostructures, the interlayer charge and energy transfer is highly efficient. Therefore, it is important to understand interlayer coupling in these materials and its role on charge and energy transfer. Here we show that in a $MoSe_2/WSe_2/WS_2$ trilayer, the interlayer coupling is strong enough to form layer-coupled states in the conduction band with the electron wavefunction extends to all three layers. Density functional theory calculations reveal that the layer-coupled states in **Q** valley are about 0.1 eV below the individual monolayer states in **K** valley, which is consistent with photoluminescence measurements. Transient absorption measurements show that these layer-coupled states provide a channel for ultrafast interlayer charge transfer between the top WS_2 and the bottom $MoSe_2$ layers. In this process, electrons from the **K** valley of the individual monolayers are scattered to the layer-coupled states in **Q** valley. Such a partial charge transfer allows formation of partial-indirect excitons with the holes in one monolayer while electrons shared by three layers. The formation of layer-coupled states is promising for harnessing emergent properties of transition metal dichalcogenide multilayer heterostructures. Our findings also provide new ingredient to understand charge and energy transfer in transition metal dichalcogenide heterobilayers, as the layer-coupled states can play important roles in the efficient transfer observed in these systems.

Graphical TOC Entry

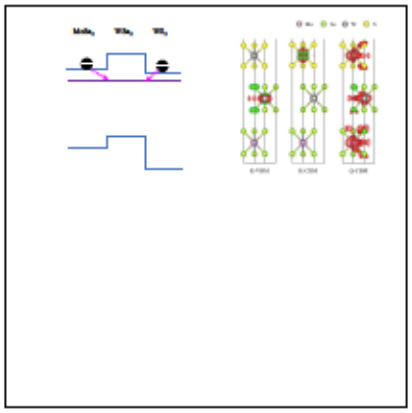

The discovery of graphene has created an exponentially growing interest in two-dimensional (2D) materials, especially transition metal dichalcogenides (TMDs).[1] These atomically thin materials possess several unique features that make them attractive to both fundamental research and applications, such as layer-dependent electronic structures,[2,3] enhanced many-body interactions,[4] and strong nonlinear optical responses.[5,6] One of the most intriguing aspects of these 2D materials is that they provide a new route to fabricate multilayer structures by combining several 2D materials[7] or with other materials[8–11] *via* van der Waals interlayer interaction. Since lattice match is no longer a constrain, a large number of materials can be chosen from to assemble multilayers with certain properties. Hence, this new approach can potentially produce a vast number of new functional materials. The interfaces in such structures are atomically sharp and the junctions can be as thin as two atomic layers - both reaching the ultimate limits. A number of drawbacks in conventional heterostructures are, at least in principle, reduced in these van der Waals multilayers, such as interfacial defects, interlayer atomic diffusion, strain, and disorders.

One key process for achieving emergent properties in van der Waals multilayers is effective transfer of charge and energy between different layers. As the first step, charge and energy transfer in heterobilayers formed by TMD and graphene have been studied by femtosecond transient absorption[12–16] and steady-state optical spectroscopy measurements.[17] Based on these studies, the following conclusions appear to be established: First, between two TMD monolayers (MLs) that form a type-II band alignment, interlayer charge transfer occurs on a time scale shorter than 100 fs.[12–15,17] Second, efficient charge transfer can occur in heterobilayers with any twist angles.[16–18] Third, energy transfer occurs on a 1-ps time scale, and makes a minor contribution when charge transfer is efficient.[17,19,20]

The observed highly efficient interlayer charge and energy transfer is encouraging news for the development of van der Waals multilayers for electronic and optoelectronic technologies. However, the physics mechanisms of charge and energy transfer are yet to be fully understood. Several theoretical models have been proposed to account for the ultrafast charge transfer

process: For example, delocalization in momentum space due to strong localization in real space may help fulfill in-plane momentum conservation requirement.[21] Quantum coherence at the interface can help overcome the Coulomb attraction.[22,23] The interlayer coupling between some states can be enhanced by the Coulomb field from initially transferred charges.[24] More recently, it was proposed that intervalley scattering of carriers from layer-uncoupled to layer-coupled states can assist charge transfer.[25] These models are plausible and have established a solid foundation for ultimate understanding of this process. However, more experimental studies that reveal different aspects of charge and energy transfer and identify dominant mechanisms under different conditions are highly desired.

Here we show that layer-coupled states are formed in a TMD trilayer, and they play a key role in ultrafast interlayer charge transfer. We found that in a $MoSe_2/WSe_2/WS_2$ trilayer, electrons can transfer from $MoSe_2$ to WS_2 on an ultrafast time scale, despite of the energy barrier of WSe_2. Even more surprisingly, electrons can also transfer efficiently from WS_2 to $MoSe_2$, despite of the fact that the **K**-valley conduction band of $MoSe_2$ is higher than WS_2. These observations indicate that the charge transfer is achieved *via* layer-coupled states that has energies lower than the individual ML states. Our density functional theory calculations show that the conduction band states in **Q** valley are coupled, lowering the energy to below the **K**-valley states by about 0.1 eV. Intervalley scattering of electrons from **K** valley of individual layers to these layer-coupled states is therefore responsible for the ultrafast partial interlayer charge transfer. These layer-coupled states are also identified in photoluminescence (PL) measurements. The formation of layer-coupled states is an important element for harnessing emergent properties of TMD multilayer heterostructures.

Figure 1(a) shows the band alignment of the $MoSe_2/WSe_2/WS_2$ trilayer sample, according to the ionization potentials and electron affinities of individual MLs from first-principle calculations.[26] That is, the individual layers are assumed to maintain their own electronic structures, without interlayer coupling. Only the **K**-valley states are plotted as they are the lowest energy states.[26] The key element of this design is that, the conduction band mini-

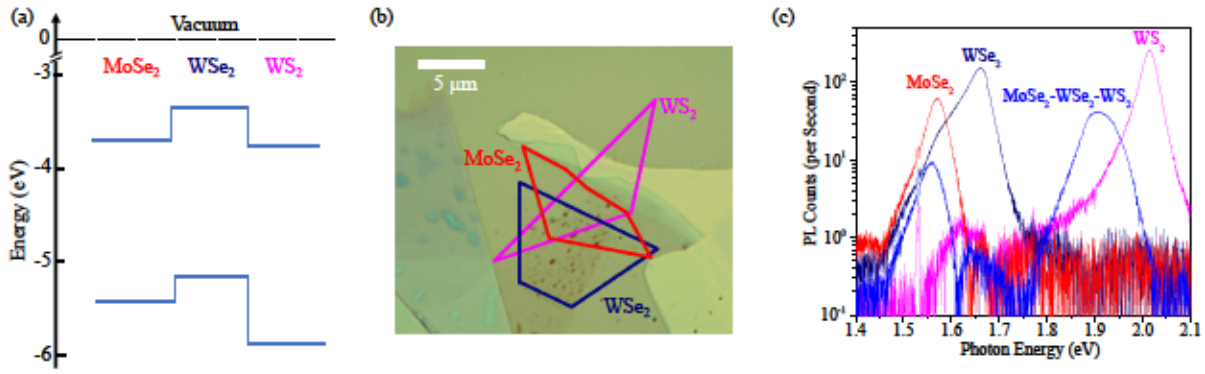

Figure 1: (a) Band alignment of the $MoSe_2/WSe_2/WS_2$ heterostructure according to the ionization potentials and electron affinities of individual monolayers from first-principle calculations.[26] (b) Microscope image of the heterostructure sample. (c) Photoluminescence spectra of the heterostructure (blue) and the three monolayers of $MoSe_2$ (red), WSe_2 (dark blue), and WS_2 (pink) obtained under the same conditions.

mum (CBM) of $MoSe_2$ is lower than WSe_2 but higher than WS_2. Hence, if only the **K**-valley states are involved, electrons excited in $MoSe_2$ could transfer to WS_2 by tunneling through the energy barrier of WSe_2, while electrons excited in WS_2 are not expected to transfer to $MoSe_2$. We note that although the magnitudes of the conduction band offsets plotted in Figure 1(a) are theoretical values,[26] it has been shown that $MoSe_2/WS_2$ forms a type-II band alignment with the CBM in WS_2,[14,19,27] while $MoSe_2/WSe_2$ also forms type-II band alignment with the CBM in $MoSe_2$.[28–30] Hence, the order of the CBM of the three materials, $WS_2 < MoSe_2 < WSe_2$, has been experimentally established. Furthermore, although slightly different theoretical values of the electron affinity of TMD MLs have been reported by different groups,[31–34] these models all agree on the above order of the CBM.

Figure 1(b) shows a microscope image of the sample used for the study, which was fabricated by mechanical exfoliation followed by dry transfer (See Supporting Information).[35–38] In addition to the trilayer region, the sample also contains regions of the three individual MLs as well as three heterobilayers. These regions facilitate their direct comparison with the trilayer. In all the measurements, the sample was kept at room temperature in ambient conditions.

To probe the quality of the sample and the interfaces, we first performed PL measure-

ments. Figure 1(c) shows the PL spectra, taken under the same conditions, of the trilayer and the three ML regions. A linearly-polarized 405-nm continuous-wave laser with a power of 100 nW was used for excitation. The PL spectra of the individual MLs - both the peak positions and the PL yields, are consistent with our previous results,[35] confirming their ML thickness. In the trilayer, the peak corresponding to $MoSe_2$ is quenched by about 7 times. This can be attributed to the transfer of photoexcited holes from $MoSe_2$ to WSe_2 and/or transfer of electrons to WS_2, before their recombination in $MoSe_2$. The quenching of the WSe_2 peak is more pronounced, about a factor of 200. No WS_2 PL can be observed in the trilayer. The observed PL quenching confirms the high quality of the interfaces of the trilayer.[14,30,39–44] A new peak at about 1.9 eV is observed in the trilayer, which is about 6 times lower than the WS_2 ML peak. At 100 meV below the WS_2 peak, no transitions between the **K**-valley states shown in Figure 1(a) can induce this peak. The origin of this peak will be discussed later in the paper.

We used a femtosecond pump-probe technique to study the dynamics of charge transfer in the heterostructures (See Supporting Information).[45] Figure 2(a) shows the pump-probe configuration intended to study electron transfer from $MoSe_2$ to WS_2. A 1.60-eV pump pulse with an energy fluence of 16 μJ cm^{-2} injects electrons (-) and holes (+) in $MoSe_2$. The estimated excited carrier density is about 4×10^{11} cm^{-2}, using an absorption coefficient[46] of 10^7 m^{-1}. Since the photon energy is smaller than the optical bandgaps of WSe_2 (1.66 eV) and WS_2 (2.01 eV), no carriers are excited in these two layers. We monitor the population of carriers in WS_2 by measuring the differential reflection of a 1.97-eV probe pulse, which is defined as the normalized change of the reflection coefficient of the sample induced by the pump, $\Delta R/R_0 = (R - R_0)/R_0$, where R and R_0 are the reflection coefficient with and without the presence of the pump beam, respectively (See Supporting Information).[45] The blue squares in Figure 2(b) and (d) show the observed differential reflection signal from the $MoSe_2/WSe_2/WS_2$ region over short (b) and long (d) time ranges. The rising part of the signal can be fit by the integral of a Gaussian function with a full-width at half maximum

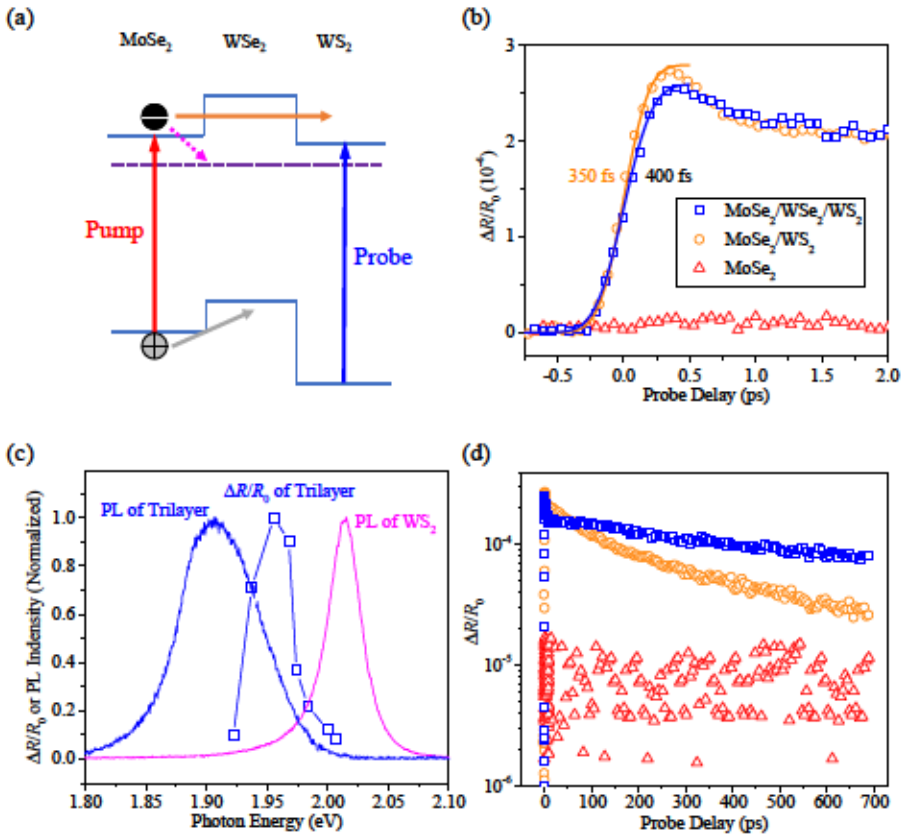

Figure 2: (a) Pump-probe configuration: A 1.60-eV pump pulse (red arrow) excites electrons (-) and holes (+) in $MoSe_2$. The holes are expected to transfer to WSe_2 (gray arrow). The electrons may tunnel to WS_2 (orange arrow) or transfer to (pink arrow) the layer-coupled states (dashed line). The possible presence of electrons in WS_2 is monitored by a 1.97-eV probe pulse (blue arrow). (b) Differential reflection signal measured from $MoSe_2/WSe_2/WS_2$ (blue squares), $MoSe_2/WS_2$ (orange circles), and $MoSe_2$ (red triangles) regions of the sample. (c) Normalized peak differential reflection signal from the trilayer region as a function of probe photon energy (black squares) and the normalized PL spectra of WS_2 ML (pink curve) and trilayer (blue curve). (d) Same as (b) but over a larger time range.

(FWHM) of 400 fs, as indicated by the blue curve over the data points. We repeated the measurement in the region of $MoSe_2/WS_2$, *i.e.* without the middle WSe_2 layer. As shown by the orange circles, the magnitude and the rising time of the signal are very similar to the trilayer, with a slightly shorter rising time corresponding to a Gaussian FWHM of 350 fs [orange curve in Figure 2(b)]. The fact that the rise times of the signal are limited by the time resolution of the setup indicates that the charge transfer times in both the trilayer and the bilayer regions are much shorter than 350 fs and the WSe_2 barrier does not influence the

transfer noticeably. The decay of the signal in the trilayer is significantly slower than the bilayer, as shown in Figure 2(d), indicating different exciton recombination dynamics.[47,48]

To understand the observed features, we first recall that the result from the $MoSe_2/WS_2$ bilayer (orange circles) is consistent with the ultrafast charge transfer process that has been observed in several TMD heterostructures.[12–15,17] Hence, the signal can be attributed to the electrons that transfer from the CB of $MoSe_2$ to that of WS_2. Since the magnitude of the signal from $MoSe_2/WSe_2/WS_2$ trilayer is similar to $MoSe_2/WS_2$, we can conclude that nearly all electrons excited in $MoSe_2$ transfer to WS_2. The similarly short rising time of the signal in trilayer shows that the electron transfer from $MoSe_2$ to WS_2 occurs on a similarly ultrafast time scale, despite of the WSe_2 energy barrier. We note that the holes are expected to transfer from $MoSe_2$ to WSe_2 on an ultrafast time scale (gray arrow), as have been observed in previous studies of $MoSe_2/WSe_2$ heterostructure.[28–30,35] Residing in the middle WSe_2 layer, these holes are not expected to contribute significantly to the signal observed.

The above interpretation is based on an assumption that the 1.97-probe, tuned to the optical bandgap of WS_2, main senses carriers in WS_2. To confirm this assumption, we repeated the measurements of the trilayer and bilayer regions on the WS_2 ML region under the same conditions. As shown by the red triangles in Figure 2(b) and (d), no signal above the noise floor was observed. This rules out the possibility that the signal was due to interaction of the probe with higher energy states in $MoSe_2$. To further confirm that the probe monitors the WS_2 layer, we measured the differential reflection signal as a function of the probe photon energy. The peak signal depends strongly on the probe photon energy in this spectral range, as shown as the blue squares in Figure 2(c). This resonant feature would not have been observed if the signal was due to the probe interacting with the other two layers. We note that for an individual WS_2 ML sample, the differential reflection signal peaks near the PL peak of WS_2 ML at about 2.00 eV, according to our previous measurements.[49] Since the differential reflection peaks at about the half-height position of the PL peak of the

trilayer (blue curve) and drops to almost zero at the PL peak, it is likely to be induced by a shift of the resonance in the trilayer that is responsible for the PL. This feature will be discussed along with the nature of the trilayer PL peak later.

The minimal effect of the WSe_2 barrier on electron transfer from $MoSe_2$ to WS_2 strongly suggests that the tunneling mechanism indicated by the orange arrow in Figure 2(a) is *not* the main channel of charge transfer. We can roughly estimate the expected tunneling time by treating this process as tunneling of an electron with an energy of 26 meV (thermal energy at room temperature) through a square energy barrier of $V_0 = 0.4$ eV (the band offset) and $L = 0.9$ nm (ML thickness). The tunneling probability $T = \{1 + [(E/V_0)(1 - E/V_0)\sinh^2(kL)]^{-1}\}^{-1}$, where $k = \sqrt{2m(V_0 - E)}/\hbar$. By using $m = 0.7m_0$, where m_0 is the rest mass of an electron,[50] we obtain $k = 2.5 \times 10^9$ /m, and therefore $T = 0.0022$. Using the velocity of the 0.026-eV electron of $v = 1.2 \times 10^5$ m s^{-1}, the rate of incidence is $R = v/2L = 0.67 \times 10^{14}$ s^{-1}. Hence, the transfer time due to tunneling is $(RT)^{-1} \approx 7$ ps, which is much longer than the observed transfer time. On the other hand, the transfer *via* layer-coupled states (the pink arrow) could explain the observed feature. In this model, we assume that some states in the CBs of the three MLs form layer-coupled states that expand across the entire trilayer. If these layer-coupled states are lower in energy, as indicated as the purple dashed line in Figure 2(a), electrons excited in the **K** valley of $MoSe_2$ can scatter to these states *via* intervalley scattering. The intervalley scattering time has been estimated as about 50 fs in TMD heterostructures,[25] which is reasonably consistent with the charge transfer time observed here.

To find more evidence on the charge transfer process *via* layer-coupled states, we next used the configuration shown in Figure 3(a). Here, the pump of 2.00 eV and 1.9 μJ cm^{-2} (red vertical arrow) excites WS_2. The excited holes are expected to transfer to WSe_2 (gray arrow). The 1.57-eV probe is tuned to the excitonic resonance of $MoSe_2$, and hence senses carriers in that layer. Since the CBM of $MoSe_2$ is *higher* than WS_2, if only the **K**-valley states are considered, the electrons are not expected to transfer to $MoSe_2$ layer. As such, observation

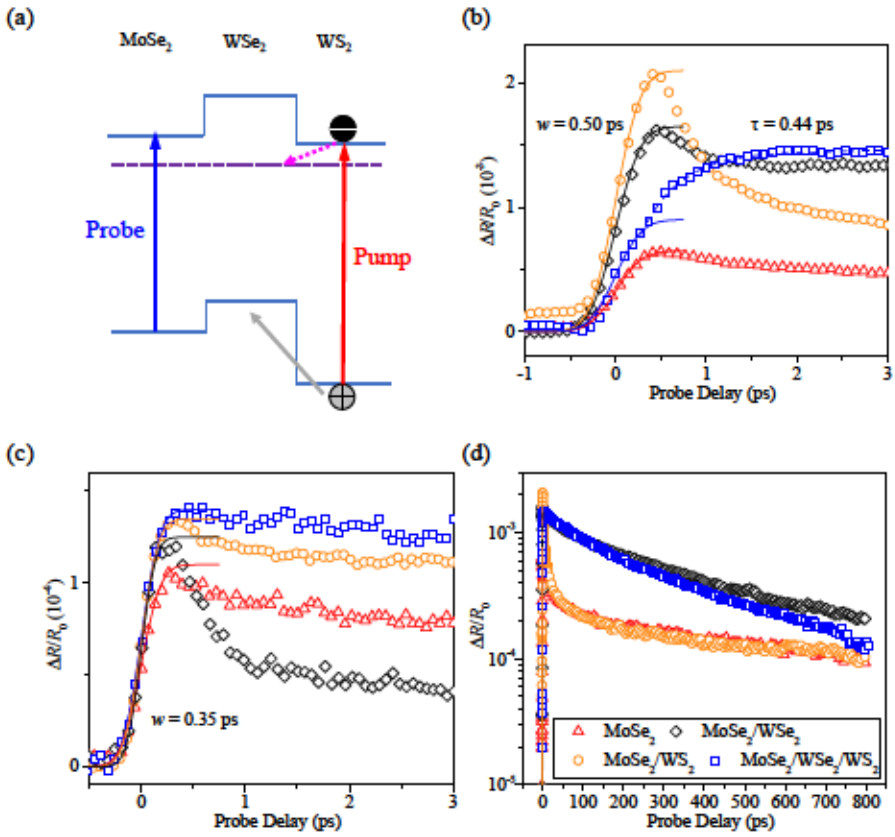

Figure 3: (a) Pump-probe configuration: A 2.00-eV pump pulse (red arrow) excites electrons (-) and holes (+) in WS_2. The holes are expected to transfer to WSe_2 (gray arrow). The electrons may transfer to the layer-coupled states (dashed line). The presence of electrons in $MoSe_2$ is monitored by a 1.57-eV probe pulse (blue arrow). (b) Differential reflection signal measured from the regions of $MoSe_2/WSe_2/WS_2$ (blue squares), $MoSe_2/WS_2$ (orange cricles), $MoSe_2/WSe_2$ (black diamonds), and $MoSe_2$ (red triangles). Curves are fits (see text). (c) Same as (b), except that a pump of 1.77 eV was used. (d) Same as (b) but over a large time range.

of electron transfer from WS_2 to $MoSe_2$ would provide evidence on the involvement of the layer-coupled states.

Unlike the configuration shown in Figure 2, where the pump only excites the targeted layer of $MoSe_2$, here, the pump inevitably excites all three layers. Hence, to separate the contributions of the directly injected carriers and transferred carriers, the same measurement was repeated on control samples of $MoSe_2$, $MoSe_2/WSe_2$, and $MoSe_2/WS_2$. The signal of $MoSe_2$ ML, shown as the red triangles in Figure 3(b) and (d), rises to a peak following the integral of a Gaussian function with a width of 0.50 ps (red curve). This time constant is

slightly longer than the instrument response time, which could be attributed to the time it takes for the initially injected hot carriers to relax to the band edges.[51,52] For $MoSe_2/WSe_2$ (black diamonds) and $MoSe_2/WS_2$ (orange circles), the rising times are also 0.50 ps (curves), confirming the ultrafast transfer of electrons from WSe_2 to $MoSe_2$ and the ultrafast hole transfer from WS_2 to $MoSe_2$, respectively.

A different time evolution of the signal was observed from the trilayer, as shown as the blue squares. The rise of the signal is significantly slower. The initial rise can still be described as the Gaussian integral of 0.5 ps (blue solid curve), and can be attributed to contributions from carriers injected in $MoSe_2$ and WSe_2. The rest of the rising can be fit by an exponential function, $\Delta R/R_0(t) = \Delta R/R_0(\infty)[1-\exp(-t/\tau)]$ (blue dashed curve), where $\Delta R/R_0(\infty)$ is the maximum value of $\Delta R/R_0$. Since carriers injected in $MoSe_2$ and WSe_2 layer are known to instantaneously produce a peak signal, the only plausible origin of the slow rise of the signal is the electrons that are excited in WS_2 and subsequently transferred to $MoSe_2$. Hence, the time constant $\tau = 0.44$ ps is attributed to the transfer time of electrons.

To further confirm the assignment of the slow-rising component to the electrons transferred from WS_2 to $MoSe_2$, we repeated this set of measurements with a 1.77-eV pump. Since the photon energy is smaller than the optical bandgap of WS_2, the pump is now unable to excite WS_2. The results are shown in Figure 3(c). As expected, without the contribution of electrons transferring from WS_2, the signal of the trilayer (black squares) rises to a peak with a time constant of 0.35 ps (black squares), just as the three control samples [Figure 3(c)]. We note that it is unlikely that carriers in WSe_2 contribute significant to the differential reflection of the 1.57-eV probe, although it also overlaps with low-energy tail of the WSe_2 exciton resonance [Figure 1(c)]. Previous spectrally resolved measurements have shown that the signal at the probe photon energy of more 40 meV below the WSe_2 optical bandgap is at least one order of magnitude lower than the signal at the optical bandgap.[53] Furthermore, hole transfer from WS_2 to WSe_2 has been found to occur on a sub-100 fs time scale,[44] much faster than the observed rising time of the signal.

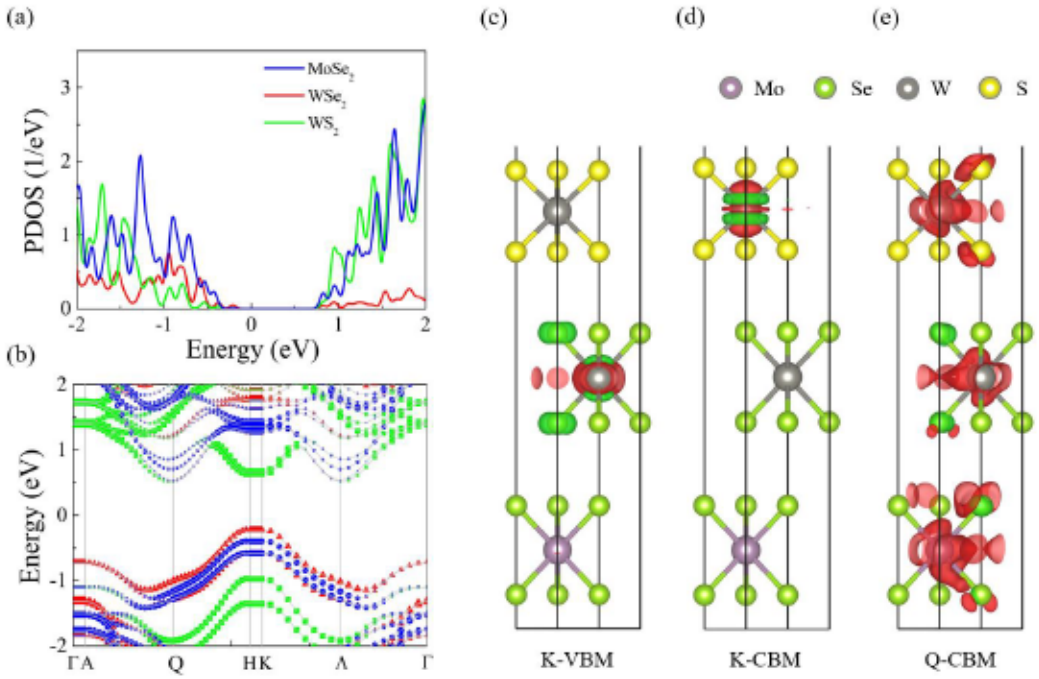

Figure 4: Projected density of states (PDOS) (a) and bandstructure (b) of the trilayer $MoSe_2/WSe_2/WS_2$ calculated using the optimized structure at the Perdew-Burke-Ernzerhof level with inclusion of the spin-orbit coupling correction. The zero energy is set to the Fermi level. The size of the symbols in (b) represents the fraction of Kohn-Sham orbital localized at the each material respectively. Charge densities (c), (d), and (e) for valance band maximum and conduction band minimum are obtained from the **K**- and **Q**-points, respectively. The iso-surface value is set to 5 $\times 10^{-4}$ e $(\text{bohr})^{-3}$.

The observed electron transfer from WS_2 to $MoSe_2$ in the trilayer sample shows clearly that the process must involve states other than **K** valley. This, along with the surprisingly fast electron transfer from $MoSe_2$ to WS_2 (despite of the WSe_2 barrier) indicate that the layer-coupled states provide a channel for such transfer, as shown as the pink arrows in Figure 3(a) and Figure 2(a). Since the wavefunctions of the electrons in these states extend to all three layers, partial presence of electrons in each layer can be sensed by probe tuned to the resonance of that layer.

We have presented strong experimental evidence that in trilayer $MoSe_2/WSe_2/WS_2$, layer-coupled states act as a channel for interlayer charge transfer. To reveal the features of these coupled states, we performed density functional theory calculations, employing the Vienna *ab initio* simulation package[54] using a converged plane-wave basis set. The gener-

alized gradient approximation of Perdew-Burke-Ernzerhof functional for electron exchange and correlation[55] and projected-augmented wave approach for electron and ion interaction[56] were used. The interlayer van der Waals interactions was described by the Grimme DFT-D3 method.[57] A 400-eV energy cutoff was used for geometry optimization and electronic structure calculations. Geometry optimization for both lattice constants and atomic coordinates with $20 \times 20 \times 1$ Γ-centered Monkhorst-Pack mesh[58] was carried out until residual forces on each atom were smaller than 0.01 eV $Å^{-1}$. A 9-atom trilayer heterostructure consisting of $MoSe_2/WSe_2/WS_2$ unit cells were built in which a 17 Å vacuum depth was added along the z axis to eliminate spurious interactions between the systems from their images. The optimized lattice constants were 3.19 Å in x and y directions. Considering strong spin-orbit coupling arising from heavy atoms, in particular Mo and W, in TMDs, the spin-orbit coupling corrections were included in the electronic property calculations.[59–61]

Figure 4(a) presents the projected density of states (PDOS) of the trilayer $MoSe_2/WSe_2/WS_2$. The PDOS is separated into contributions from $MoSe_2$ (blue), WSe_2 (red) and WS_2 (green), respectively. The VBM of the trilayer is composed primarily by WSe_2 layer, while the CBM originates from the mixing states from all three layers. Figure 4(b) shows the band-structure that further confirms the energy alignment analysis from the PDOS and gives the more subtle features of electronic structure. Similar to TMD MLs, the VBM of the trilayer $MoSe_2/WSe_2/WS_2$ remains at the **K** point. The CBM, however, moves to the lower energy **Q** point because the coupled states formed by the three MLs push it down and result in the **Q**/Λ states lower than all the **K** states. We note that similar phenomena have been found in few-layer $MoSe_2$ and bilayer MoS_2.[25,62] As a more straightforward proof, while the charge densities of VBM and CBM calculated at **K**-point are localized at WSe_2 and WS_2 respectively [Figure 4(c) and 4(d)], the CBM at **Q**-point is delocalized among all three layers and forms a strongly couple state [Figure 4(e)]. Hence, scattering of electrons from **K** valley of any ML to the layer-coupled states in **Q** valley gives rise to interlayer charge transfer, with a transfer time determined by the intervalley scattering time. It is interesting to note that

while the electron transfer from $MoSe_2$ to WS_2 is faster than our time resolution, the transfer time from WS_2 to $MoSe_2$ is 0.44 ps. The difference could be attributed to the difference in intervalley scattering rates in the two situations. However, further studies are necessary to fully account for this feature.

Results shown in Fig. 4 are based on a single particle approach. Since in TMD MLs, the Coulomb effects are strong, it is interesting to check whether such effects can alter the results significantly. We repeated the PDOS and bandstructure calculations for the trilayer at the GW level containing spin-orbit interactions. The results (See Supporting Information) show that the energy alignment does not change. Furthermore, to check whether the 17-Å vacuum depth is sufficient to screen spurious interactions, we repeated the PDOS, bandstructure, and charge density calculations at the PBE level containing spin-orbit coupling using the same system, but with 15-and 20-Å vacuum depths, respectively. The results are provided in Supporting Information. The energy alignment, valley alignment between **Q** and **K**, and charge localization remain largely unchanged compared to the results of 17-Å vacuum depth. Hence, the choice of 17-Å vacuum depth achieves a reasonable balance between the computational cost and the data convergence.

The layer-coupled states obtained in the calculation are also consistent with PL spectrum of the trilayer. According to Figure 4(b), the layer-coupled states in **Q** valley is about 0.1 eV lower than the **K** valley of WS_2 ML. The PL peak of the trilayer shown in Figure 1(c) is lower than the peak of WS_2 ML by the same amount. Hence, we can attribute the PL peak of the trilayer at 1.9 eV to the recombination of excitons with the electrons in the layer-coupled **Q** valley and holes in the **K** valley of WS_2. It is interesting to note that the measurement was performed with the sample at room temperature. The rather strong PL emission from interlayer excitons observed here could be attributed to partial overlap of the wavefunctions of electrons and holes, since a significant portion of the electron wavefunction in **Q** valley is in WS_2 layer. We note that trions in WS_2 could have contributions to this peak too, since charge transfer can facilitate formation of trions. However, since the trion binding energy in

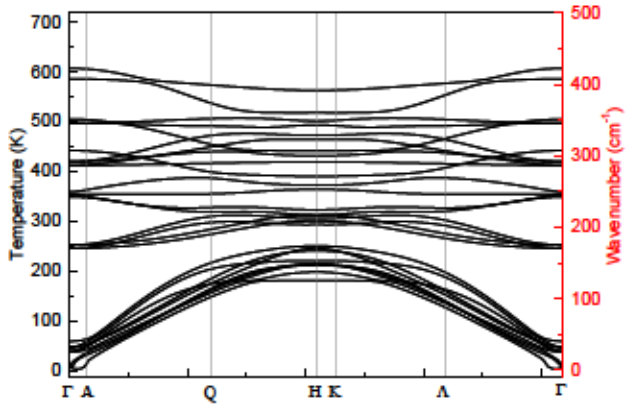

Figure 5: Calculated phonon spectrum of the $MoSe_2/WSe_2/WS_2$ trilayer.

WS_2 was found to be in the range of 10 - 40 meV in previous studies,[63–66] their contribution is likely limited to the high-energy side of this peak. Furthermore, as shown in Figure 2(c), the differential reflection signal is peaked when the probe photon energy is between the two PL peaks. This could be indicative that the probe senses the electrons in the layer-coupled states *via* interacting with both transitions.

Scattering of electrons from **K** to **Q** valleys requires involvement of phonons to conserve crystal momentum.[67,68] In order to identify which phonon modes participate in these processes, we calculated the phonon spectrum of the trilayer $MoSe_2/WSe_2/WS_2$. As shown in Fig. 5, there is no imaginary frequencies, further confirming that the trilayer is stable. According to the spectrum, only the modes below 200 cm^{-1} can be populated at room temperature, which create electron-phonon coupling and promote the intervalley electrons relaxation and radiative recombination.

Previously, interlayer excitons, or charge-transfer excitons, in TMD heterostructures have been extensively studied. In these excitons, the electrons and holes are located in different layers. Due to the small overlap of the electron and hole wavefunctions, these excitons have shown very long lifetimes.[13,14,21,28,30,69–72] In the trilayer studied here, after the charge transfer, excitons can also form between the electrons in the layer-coupled states and the holes in WSe_2. Differing from the previously studied interlayer indirect excitons, these can be called as partially indirect excitons since there is partially overlap of electron and hole

wavefunctions, which might facilitate their recombination. On the other hand, however, the momentum mismatch between electrons and holes would reduce their recombination rate. The long-term decay of the differential reflection signal shown in Figure 2(d) can be attributed to the lifetime of these excitons. The comparison of the blue and orange symbols in Figure 2(d) suggests that the lifetime of the excitons in the trilayer is longer than the interlayer excitons in the $MoSe_2/WS_2$ bilayer.

In conclusion, we have shown that in a $MoSe_2/WSe_2/WS_2$ trilayer heterostructure, the interlayer coupling for states in the **Q** valley is strong enough to form coupled states in the CB that are about 0.1 eV below the lowest **K**-valley states. These layer-coupled states provide a channel for interlayer charge transfer between the top WS_2 and the bottom $MoSe_2$ layers, despite of the energy barrier of the middle WSe_2 layer. Partial charge transfer is achieved *via* intervalley scattering of electrons from the **K** valley of one individual layer to the layer-coupled states in **Q** valley, as the wavefunctions of the electron in these states extend to all three layers. The formation of layer-coupled states is an important element for harnessing emergent properties of TMD multilayer heterostructures. The findings also provide new ingredients for understanding ultrafast charge and energy transfer in TMD heterobilayers that has been previously studies, as the layer-coupled states can play an important role in the efficient transfer observed in these systems.

Acknowledgment

This material is based upon work supported by the National Science Foundation of USA (No. DMR-1505852). R. L. acknowledges the National Science Foundation of China, grant Nos. 51861135101 and 21573022, and the Fundamental Research Funds for the Central Universities. P.Z. and Y.W. contributed equally to this work.

Supporting Information Available

The following files are available free of charge.

Experimental techniques and procedures, numerical results with different vacuum depths, GW results.

References

(1) Lin, Z.; McCreary, A.; Briggs, N.; Subramanian, S.; Zhang, K. H.; Sun, Y. F.; Li, X. F.; Borys, N. J.; Yuan, H. T.; Fullerton-Shirey, S. K. et al. 2D Materials Advances: From Large Scale Synthesis and Controlled Heterostructures to Improved Characterization Techniques, Defects and Applications. *2D Mater.* **2016**, *3*, 042001.

(2) Splendiani, A.; Sun, L.; Zhang, Y.; Li, T.; Kim, J.; Chim, C. Y.; Galli, G.; Wang, F. Emerging Photoluminescence in Monolayer MoS_2. *Nano Lett.* **2010**, *10*, 1271–1275.

(3) Mak, K. F.; Lee, C.; Hone, J.; Shan, J.; Heinz, T. F. Atomically Thin MoS_2: A New Direct-Gap Semiconductor. *Phys. Rev. Lett.* **2010**, *105*, 136805.

(4) He, K.; Kumar, N.; Zhao, L.; Wang, Z.; Mak, K. F.; Zhao, H.; Shan, J. Tightly Bound Excitons in Monolayer WSe_2. *Phys. Rev. Lett.* **2014**, *113*, 026803.

(5) Kumar, N.; Najmaei, S.; Cui, Q.; Ceballos, F.; Ajayan, P. M.; Lou, J.; Zhao, H. Second Harmonic Microscopy of Monolayer MoS_2. *Phys. Rev. B* **2013**, *87*, 161403.

(6) Autere, A.; Ryder, C. R.; Saynatjoki, A.; Karvonen, L.; Amirsolaimani, B.; Norwood, R. A.; Peyghambarian, N.; Kieu, K.; Lipsanen, H.; Hersam, M. C. et al. Rapid and Large-Area Characterization of Exfoliated Black Phosphorus Using Third-Harmonic Generation Microscopy. *J. Phys. Chem. Lett.* **2017**, *8*, 1343–1350.

(7) Geim, A. K.; Grigorieva, I. V. Van der Waals Heterostructures. *Nature* **2013**, *499*, 419–425.

(8) Fang, Q. Y.; Shang, Q. Y.; Zhao, L. Y.; Wang, R.; Zhang, Z. P.; Yang, P. F.; Sui, X. Y.; Qiu, X. H.; Liu, X. F.; Zhang, Q. et al. Ultrafast Charge Transfer in Perovskite Nanowire/2D Transition Metal Dichalcogenide Heterostructures. *J. Phys. Chem. Lett.* **2018**, *9*, 1655–1662.

(9) Goodman, A. J.; Dahod, N. S.; Tisdale, W. A. Ultrafast Charge Transfer at a Quantum Dot/2D Materials Interface Probed by Second Harmonic Generation. *J. Phys. Chem. Lett.* **2018**, *9*, 4227–4232.

(10) Kafle, T.; Kattel, B.; Lane, S. D.; Wang, T.; Zhao, H.; Chan, W. L. Charge Transfer Exciton and Spin Flipping at Organic-Transition Metal Dichalcogenide Interfaces. *ACS Nano* **2017**, *11*, 10184–10192.

(11) Zhong, C. M.; Sangwan, V. K.; Wang, C.; Bergeron, H.; Hersam, M. C.; Weiss, E. A. Mechanisms of Ultrafast Charge Separation in a PTB7/Monolayer MoS_2 van der Waals Heterojunction. *J. Phys. Chem. Lett.* **2018**, *9*, 2484–2491.

(12) Hong, X.; Kim, J.; Shi, S. F.; Zhang, Y.; Jin, C.; Sun, Y.; Tongay, S.; Wu, J.; Zhang, Y.; Wang, F. Ultrafast Charge Transfer in Atomically Thin MoS_2/WS_2 Heterostructures. *Nat. Nanotechnol.* **2014**, *9*, 682–686.

(13) Ceballos, F.; Bellus, M. Z.; Chiu, H. Y.; Zhao, H. Ultrafast Charge Separation and Indirect Exciton Formation in a MoS_2-$MoSe_2$ van der Waals Heterostructure. *ACS Nano* **2014**, *8*, 12717–12724.

(14) Ceballos, F.; Bellus, M. Z.; Chiu, H. Y.; Zhao, H. Probing Charge Transfer Excitons in a $MoSe_2$-WS_2 van der Waals Heterostructure. *Nanoscale* **2015**, *7*, 17523–17528.

(15) Peng, B.; Yu, G.; Liu, X.; Liu, B.; Liang, X.; Bi, L.; Deng, L.; Sum, T. C.; Loh, K. P. Ultrafast Charge Transfer in MoS_2/WSe_2 P-N Heterojunction. *2D Mater.* **2016**, *3*, 025020.

(16) Zhu, H. M.; Wang, J.; Gong, Z. Z.; Kim, Y. D.; Hone, J.; Zhu, X. Y. Interfacial Charge Transfer Circumventing Momentum Mismatch at Two-Dimensional Van Der Waals Heterojunctions. *Nano Lett.* **2017**, *17*, 3591–3598.

(17) Rigos, A. F.; Hill, H. M.; Li, Y. L.; Chernikov, A.; Heinz, T. F. Probing Interlayer Interactions in Transition Metal Dichalcogenide Heterostructures by Optical Spectroscopy: MoS_2/WS_2 and $MoSe_2/WSe_2$. *Nano Lett.* **2015**, *15*, 5033–5038.

(18) Schaibley, J. R.; Rivera, P.; Yu, H. Y.; Seyler, K. L.; Yan, J. Q.; Mandrus, D. G.; Taniguchi, T.; Watanabe, K.; Yao, W.; Xu, X. D. Directional Interlayer Spin-Valley Transfer in Two-Dimensional Heterostructures. *Nat. Commun.* *7*, 13747.

(19) Kozawa, D.; Carvalho, A.; Verzhbitskiy, I.; Giustiniano, F.; Miyauchi, Y.; Mouri, S.; Neto, A. H. C.; Matsuda, K.; Eda, G. Evidence for Fast Interlayer Energy Transfer in $MoSe_2/WS_2$ Heterostructures. *Nano Lett.* **2016**, *16*, 4087–4093.

(20) Bellus, M. Z.; Li, M.; Lane, S.; Ceballos, F.; Cui, Q.; Zeng, X. C.; Zhao, H. Type-I van der Waals Heterostructure Formed by MoS_2 and ReS_2 Monolayers. *Nanoscale Horiz.* **2016**, *2*, 31–36.

(21) Zhu, X.; Monahan, N. R.; Gong, Z.; Zhu, H.; Williams, K. W.; Nelson, C. A. Charge Transfer Excitons at van der Waals Interfaces. *J. Am. Chem. Soc.* **2015**, *137*, 8313–8320.

(22) Long, R.; Prezhdo, O. V. Quantum Coherence Facilitates Efficient Charge Separation at a $MoS_2/MoSe_2$ van der Waals Junction. *Nano Lett.* **2016**, *16*, 1996–2003.

(23) Yang, Y. T.; Fang, W. H.; Long, R. Disparity in Photoexcitation Dynamics between Vertical and Lateral MoS_2/WSe_2 Heterojunctions: Time-Domain Simulation Emphasizes the Importance of Donor Acceptor Interaction and Band Alignment. *J. Phys. Chem. Lett.* **2017**, *8*, 5771–5778.

(24) Wang, H.; Bang, J.; Sun, Y. Y.; Liang, L. B.; West, D.; Meunier, V.; Zhang, S. B. The Role of Collective Motion in the Ultrafast Charge Transfer in van der Waals Heterostructures. *Nat. Commun.* **2016**, *7*, 11504.

(25) Wang, Y.; Wang, Z.; Yao, W.; Liu, G. B.; Yu, H. Y. Interlayer Coupling in Commensurate and Incommensurate Bilayer Structures of Transition-Metal Dichalcogenides. *Phys. Rev. B* **2017**, *95*, 115429.

(26) Guo, Y. Z.; Robertson, J. Band Engineering in Transition Metal Dichalcogenides: Stacked *Versus* Lateral Heterostructures. *Appl. Phys. Lett.* **2016**, *108*, 233104.

(27) Keyshar, K.; Berg, M.; Zhang, X.; Vajtai, R.; Gupta, G.; Chan, C. K.; Beechem, T. E.; Ajayan, P. M.; Mohite, A. D.; Ohta, T. Experimental Determination of the Ionization Energies of $MoSe_2$, WS_2, and MoS_2 on SiO_2 Using Photoemission Electron Microscopy. *ACS Nano* **2017**, *11*, 8223–8230.

(28) Ross, J. S.; Rivera, P.; Schaibley, J.; Lee-Wong, E.; Yu, H. Y.; Taniguchi, T.; Watanabe, K.; Yan, J. Q.; Mandrus, D.; Cobden, D. et al. Interlayer Exciton Optoelectronics in a 2D Heterostructure P-N Junction. *Nano Lett.* **2017**, *17*, 638–643.

(29) Nayak, P. K.; Horbatenko, Y.; Ahn, S.; Kim, G.; Lee, J. U.; Ma, K. Y.; Jang, A. R.; Lim, H.; Kim, D.; Ryu, S. et al. Probing Evolution of Twist-Angle-Dependent Interlayer Excitons in $MoSe_2/WSe_2$ van der Waals Heterostructures. *Acs Nano* **2017**, *11*, 4041–4050.

(30) Rivera, P.; Schaibley, J. R.; Jones, A. M.; Ross, J. S.; Wu, S.; Aivazian, G.; Klement, P.; Seyler, K.; Clark, G.; Ghimire, N. J. et al. Observation of Long-Lived Interlayer Excitons in Monolayer $MoSe_2$-WSe_2 Heterostructures. *Nat. Commun.* **2015**, *6*, 6242.

(31) Kang, J.; Tongay, S.; Zhou, J.; Li, J. B.; Wu, J. Q. Band Offsets and Heterostructures of Two-Dimensional Semiconductors. *Appl. Phys. Lett.* **2013**, *102*, 012111.

(32) Gong, C.; Zhang, H. J.; Wang, W. H.; Colombo, L.; Wallace, R. M.; Cho, K. J. Band Alignment of Two-Dimensional Transition Metal Dichalcogenides: Application in Tunnel Field Effect Transistors. *Appl. Phys. Lett.* **2013**, *103*, 053513.

(33) Amin, B.; Singh, N.; Schwingenschlogl, U. Heterostructures of Transition Metal Dichalcogenides. *Phys. Rev. B* **2015**, *92*, 075439.

(34) Ozcelik, V. O.; Azadani, J. G.; Yang, C.; Koester, S. J.; Low, T. Band Alignment of Two-Dimensional Semiconductors for Designing Heterostructures with Momentum Space Matching. *Phys. Rev. B* **2016**, *94*, 035125.

(35) Ceballos, F.; Zereshki, P.; Zhao, H. Separating Electrons and Holes by Monolayer Increments in van der Waals Heterostructures. *Phys. Rev. Mater.* **2017**, *1*, 044001.

(36) Ceballos, F.; Ju, M. G.; Lane, S. D.; Zeng, X. C.; Zhao, H. Highly Efficient and Anomalous Charge Transfer in van der Waals Trilayer Semiconductors. *Nano Lett.* **2017**, *17*, 1623–1628.

(37) Li, Y. Y.; Cui, Q. N.; Ceballos, F.; Lane, S. D.; Qi, Z. M.; Zhao, H. Ultrafast Interlayer Electron Transfer in Incommensurate Transition Metal Dichalcogenide Homobilayers. *Nano Lett.* **2017**, *17*, 6661–6666.

(38) Samuel, D. L.; Hui, Z. Unipolar Optical Doping and Extended Photocarrier Lifetime in Graphene by Band-Alignment Engineering. *Nano Futures* **2018**, *2*, 035003.

(39) Fang, H.; Battaglia, C.; Carraro, C.; Nemsak, S.; Ozdol, B.; Kang, J. S.; Bechtel, H. A.; Desai, S. B.; Kronast, F.; Unal, A. A. et al. Strong Interlayer Coupling in van der Waals Heterostructures Built From Single-Layer Chalcogenides. *Proc. Natl. Acad. Sci. U. S. A.* **2014**, *111*, 6198–6202.

(40) Lee, C. H.; Lee, G. H.; van der Zande, A. M.; Chen, W.; Li, Y.; Han, M.; Cui, X.;

Arefe, G.; Nuckolls, C.; Heinz, T. F. et al. Atomically Thin P-N Junctions with van der Waals Heterointerfaces. *Nat. Nanotechnol.* **2014**, *9*, 676–681.

(41) Furchi, M. M.; Pospischil, A.; Libisch, F.; Burgdorfer, J.; Mueller, T. Photovoltaic Effect in an Electrically Tunable van der Waals Heterojunction. *Nano Lett.* **2014**, *14*, 4785–4791.

(42) Tongay, S.; Fan, W.; Kang, J.; Park, J.; Koldemir, U.; Suh, J.; Narang, D. S.; Liu, K.; Ji, J.; Li, J. et al. Tuning Interlayer Coupling in Large-Area Heterostructures with CVD-Grown MoS_2 and WS_2 Monolayers. *Nano Lett.* **2014**, *14*, 3185–3190.

(43) Bellus, M. Z.; Ceballos, F.; Chiu, H.-Y.; Zhao, H. Tightly Bound Trions in Transition Metal Dichalcogenide Heterostructures. *ACS Nano* **2015**, *9*, 6459–6464.

(44) Wang, K.; Huang, B.; Tian, M.; Ceballos, F.; Lin, M.-W.; Mahjouri-Samani, M.; Boulesbaa, A.; Puretzky, A. A.; Rouleau, C. M.; Yoon, M. et al. Interlayer Coupling in Twisted WSe_2/WS_2 Bilayer Heterostructures Revealed by Optical Spectroscopy. *ACS Nano* **2016**, *10*, 6612–6622.

(45) Ceballos, F.; Zhao, H. Ultrafast Laser Spectroscopy of Two-Dimensional Materials beyond Graphene. *Adv. Funct. Mater.* **2017**, *27*, 1604509.

(46) Liu, H.-L.; Shen, C.-C.; Su, S.-H.; Hsu, C.-L.; Li, M.-Y.; Li, L.-J. Optical Properties of Monolayer Transition Metal Dichalcogenides Probed by Spectroscopic Ellipsometry. *Appl. Phys. Lett.* **2014**, *105*, 201905.

(47) Li, L. Q.; Long, R.; Bertolini, T.; Prezhdo, O. V. Sulfur Adatom and Vacancy Accelerate Charge Recombination in MoS_2 but by Different Mechanisms: Time-Domain Ab Initio Analysis. *Nano Lett.* **2017**, *17*, 7962–7967.

(48) Li, L.; Long, R.; Prezhdo, O. V. Why Chemical Vapor Deposition Grown MoS_2 Sam-

ples Outperform Physical Vapor Deposition Samples: Time-Domain ab Initio Analysis. *Nano Lett.* **2018**, *18*, 4008–4014.

(49) He, J.; Kumar, N.; Bellus, M. Z.; Chiu, H. Y.; He, D.; Wang, Y.; Zhao, H. Electron Transfer and Coupling in Graphene-Tungsten Disulfide van der Waals Heterostructures. *Nat. Commun.* **2014**, *5*, 5622.

(50) Ramasubramaniam, A. Large excitonic effects in monolayers of molybdenum and tungsten dichalcogenides. *Phys. Rev. B* **2012**, *86*, 115409.

(51) Nie, Z.; Long, R.; Sun, L.; Huang, C. C.; Zhang, J.; Xiong, Q.; Hewak, D. W.; Shen, Z.; Prezhdo, O. V.; Loh, Z. H. Ultrafast Carrier Thermalization and Cooling Dynamics in Few-Layer MoS_2. *ACS Nano* **2014**, *8*, 10931–10940.

(52) Nie, Z. G.; Long, R.; Teguh, J. S.; Huang, C. C.; Hewak, D. W.; Yeow, E. K. L.; Shen, Z. X.; Prezhdo, O. V.; Loh, Z. H. Ultrafast Electron and Hole Relaxation Pathways in Few-Layer MoS_2. *J. Phys. Chem. C* **2015**, *119*, 20698–20708.

(53) Cui, Q.; Ceballos, F.; Kumar, N.; Zhao, H. Transient absorption microscopy of monolayer and bulk WSe_2. *ACS Nano* **2014**, *8*, 2970–2976.

(54) Kresse, G.; Furthmüller, J. Efficient Iterative Schemes for *Ab Initio* Total-Energy Calculations Using a Plane-Wave Basis Set. *Phys. Rev. B* **1996**, *54*, 11169–11186.

(55) Perdew, J. P.; Burke, K.; Ernzerhof, M. Generalized Gradient Approximation Made Simple. *Phys. Rev. Lett.* **1996**, *77*, 3865–3868.

(56) Blöchl, P. E. Projector Augmented-Wave Method. *Phys. Rev. B* **1994**, *50*, 17953–17979.

(57) Grimme, S.; Antony, J.; Ehrlich, S.; Krieg, H. A consistent and accurate *ab initio* parametrization of density functional dispersion correction (DFT-D) for the 94 elements H-Pu. *J. Chem. Phys.* **2010**, *132*, 154104.

(58) Monkhorst, H. J.; Pack, J. D. Special Points for Brillouin-Zone Integrations. *Phys. Rev. B* **1976**, *13*, 5188–5192.

(59) Zhu, Z. Y.; Cheng, Y. C.; Schwingenschlögl, U. Giant Spin-Orbit-Induced Spin Splitting in Two-Dimensional Transition-Metal Dichalcogenide Semiconductors. *Phys. Rev. B* **2011**, *84*, 153402.

(60) Liu, G.-B.; Shan, W.-Y.; Yao, Y.; Yao, W.; Xiao, D. Three-Band Tight-Binding Model for Monolayers of Group-Vib Transition Metal Dichalcogenides. *Phys. Rev. B* **2013**, *88*, 085433.

(61) Kosmider, K.; Gonzalez, J. W.; Fernandez-Rossier, J. Large spin splitting in the conduction band of transition metal dichalcogenide monolayers. *Phys. Rev. B* **2013**, *88*, 245436.

(62) Bradley, A. J.; Ugeda, M. M.; da Jornada, F. H.; Qiu, D. Y.; Ruan, W.; Zhang, Y.; Wickenburg, S.; Riss, A.; Lu, J.; Mo, S. K. et al. Probing the Role of Interlayer Coupling and Coulomb Interactions on Electronic Structure in Few-Layer $MoSe_2$ Nanostructures. *Nano Lett.* **2015**, *15*, 2594–2599.

(63) Shang, J. Z.; Shen, X. N.; Cong, C. X.; Peimyoo, N.; Cao, B. C.; Eginligil, M.; Yu, T. Observation of Excitonic Fine Structure in a 2D Transition-Metal Dichalcogenide Semiconductor. *ACS Nano* **2015**, *9*, 647–655.

(64) Currie, M.; Hanbicki, A. T.; Kioseoglou, G.; Jonker, B. T. Optical Control of Charged Exciton States in Tungsten Disulfide. *Appl. Phys. Lett.* **2015**, *106*.

(65) Boulesbaa, A.; Huang, B.; Wang, K.; Lin, M. W.; Mahjouri-Samani, M.; Rouleau, C.; Xiao, K.; Yoon, M.; Sumpter, B.; Puretzky, A. et al. Observation of Two Distinct Negative Trions in Tungsten Disulfide Monolayers. *Phys. Rev. B* **2015**, *92*, 115443.

(66) Mitioglu, A. A.; Plochocka, P.; Jadczak, J. N.; Escoffier, W.; Rikken, G.; Kulyuk, L.; Maude, D. K. Optical Manipulation of the Exciton Charge State in Single-Layer Tungsten Disulfide. *Phys. Rev. B* **2013**, *88*, 245403.

(67) Zheng, Q. J.; Saidi, W. A.; Xie, Y.; Lan, Z. G.; Prezhdo, O. V.; Petek, H.; Zhao, J. Phonon-Assisted Ultrafast Charge Transfer at van der Waals Heterostructure Interface. *Nano Lett.* **2017**, *17*, 6435–6442.

(68) Zheng, Q. J.; Xie, Y.; Lan, Z. G.; Prezhdo, O. V.; Saidi, W. A.; Zhao, J. Phonon-Coupled Ultrafast Interlayer Charge Oscillation at van der Waals Heterostructure Interfaces. *Phys. Rev. B* **2018**, *97*, 205417.

(69) Yu, Y. F.; Hu, S.; Su, L. Q.; Huang, L. J.; Liu, Y.; Jin, Z. H.; Purezky, A. A.; Geohegan, D. B.; Kim, K. W.; Zhang, Y. et al. Equally Efficient Inter Layer Exciton Relaxation and Improved Absorption in Epitaxial and Nonepitaxial MoS_2/WS_2 Heterostructures. *Nano Lett.* **2015**, *15*, 486–491.

(70) Nayak, P. K.; Horbatenko, Y.; Ahn, S.; Kim, G.; Lee, J. U.; Ma, K. Y.; Jang, A. R.; Lim, H.; Kim, D.; Ryu, S. et al. Probing Evolution of Twist-Angle-Dependent Interlayer Excitons in $MoSe_2/WSe_2$ van Der Waals Heterostructures. *ACS Nano* **2017**, *11*, 4041–4050.

(71) Miller, B.; Steinhoff, A.; Pano, B.; Klein, J.; Jahnke, F.; Holleitner, A.; Wurstbauer, U. Long-Lived Direct and Indirect Interlayer Excitons in van der Waals Heterostructures. *Nano Lett.* **2017**, *17*, 5229–5237.

(72) Latini, S.; Winther, K. T.; Olsen, T.; Thygesen, K. S. Interlayer Excitons and Band Alignment in MoS_2/hBN/WSe_2 van der Waals Heterostructures. *Nano Lett.* **2017**, *17*, 938–945.